Efficient rigorous calculations of power flow in grating coupled surface-emitting devices

M. G. Moharam and Andrew B. Greenwell
School of Optics/CREOL, University of Central Florida, Orlando FL 32816-2700

ABSTRACT

We present an extremely efficient rigorous vector electromagnetic analysis of field distribution and power flow in grating coupled surface emitting structures. The developed technique is based on constructing an artificially periodic structure of identical grating coupled device cells separated by anisotropic magnetic/electric perfect matching layers. The resulting periodic multi-layered structure is analyzed using the RCWA combined with a very efficient scattering matrix recursive technique. Calculated distributions of the electric and magnetic field components within the structure as well as the fields coupled into the output regions and into the substrate for typical devices are presented. Field distribution and power flow in the longitudinal and in the transverse directions in the structure are determined for the first time to our knowledge.

Keywords: Grating couplers, grating diffraction.

1. INTRODUCTION

Semiconductor lasers are the source of choice in applications ranging from telecommunications, medicine, and consumer electronics. They are very efficient, compact, low cost, and easily integrated in various systems. Standard Fabry-Perot (FP) semiconductor lasers have excellent mode quality and are suitable for in-plane integration but suffer from a highly astigmatic beam that requires active alignment of external optics. Vertical-cavity surface- emitting lasers (VCSEL) offer the possibility of superior beam quality, in a low cost light source but suffer from low power and less desirable mode behavior. Grating out-coupled surface-emitting lasers and optical amplifiers combine the surface emission and beam quality of VCSELs and the superior mode quality and in-line integration of Fabry-Perot (FP) lasers [1,2]. They also offer the potential of 10-50 times the maximum operating power of FP lasers. In these structures a diffraction grating is patterned and etched in the p-doped layer of a laser diode. The grating couples the guided mode to radiating modes in the air and in the substrate. The large emitting area combined with wide-stripe gain geometries also enables high power with higher threshold for catastrophic optical damage.

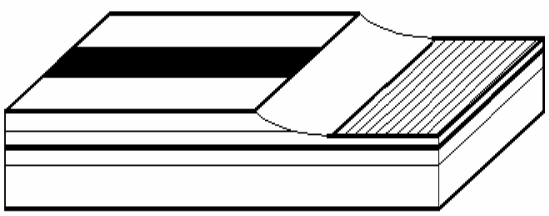

Fig. 1. Grating-coupled surface-emitting lasers

1.1 Definition of the Problem:

Semiconductor laser diodes and laser amplifier devices are formed of a doped multi-quantum well semiconductor gain layer within a lower index lossless region for mode confinement. The grating coupler section is fabricated by patterning and etching a diffraction grating in the surface of the structure. As the mode in the active (gain) region of the structure propagates into the region with etched grating, energy is gradually coupled out of the structure into the air region and into the substrate region. In addition, the discontinuity at the interface between the two regions causes energy to be reflected back in the active gain region as shown in fig. 2. The depth, duty cycle, and periodicity of the grating

Photon Management, edited by Frank Wyrowski, Proceedings of SPIE Vol. 5456
(SPIE, Bellingham, WA, 2004) · 0277-786X/04/$15 · doi: 10.1117/12.549477

structure significantly impact the fraction of energy coupled into the air and into the substrate, the rate of coupling, and therefore, the spatial profile of the output beam. The problem under consideration to profile is to analyze the structure accurately to determine its surface coupling characteristics as well as the energy reflected back into the laser amplifier that may negatively impact and/or limit its operation. Modelling this structure requires full rigorous solution of the electromagnetic boundary value problem to determine the field distribution within the structure, in order to account for the interaction between the two sections (the waveguide section and the coupler section) and the out-coupling in both air and substrate regions.

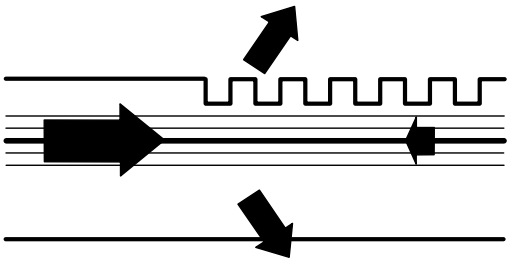

Fig. 2. Schematic of grating-coupled surface-emitting lasers

Most of the earlier published work on scattering by dielectric couplers involves determining a complex propagation constant for the leaky mode in a grating coupler region of infinite length. The imaginary part of the propagation constant describes the rate of exponential decay of the field as it propagates in the coupler, giving a measure of the output coupling efficiency. The coupled field therefore has an exponential profile. This approach does not account for the mode transition at the discontinuous boundary between the waveguide region and the coupler.

Typical semiconductor laser and optical amplifiers operate in the range of 800-1500 nm. Semiconductor materials have high index (n>3) and a typical grating coupler period is around the wavelength in the semiconductors (one third of a wavelength or ~300 nm). For sufficient coupling over a reasonable coupler length, the etched grating is relatively deep (~250nm). The coupler length is typically 250-1000 microns. This requires a very accurate modeling technique that is based on the exact solution of the Maxwell's equations, and a full vector electromagnetic representation of the optical field distribution in the structure must be used. However, the high index contrast and the small features over a large area present a significant challenge. Standard analysis techniques that are based on the calculation of electromagnetic fields on a spatial grid such as Finite Difference Time Domain (FDTD) method, method of moments, and similar techniques have been used to analyze many structures. However, the large length and small features (~150 nm) of the grating coupler necessitate an extremely fine grid over a large area to obtain useful accurate results. These requirements make these grid-based techniques prohibitively inefficient to be of practical use for analyzing these structures.

In this work, we present an extremely efficient rigorous vector electromagnetic analysis of the field distribution and power flow in grating coupled surface emitting structures, specifically amplifier. The developed technique is based on constructing an artificially periodic structure of identical grating coupled device cells separated by anisotropic magnetic/electric perfect matching layers. The resulting periodic multi-layered structure is analyzed using the RCWA. A very efficient implementation of the S-matrix recursive approach is developed to overcome the numerical inefficiency associated with up to 4,000 layers in the grating structure. Calculated field distribution, mode structure, and output coupled fields are presented. Execution time using a 2.5 GHz Pentium 4 PC is less than 30 seconds. We present calculated distributions of all the electric and magnetic field components within the structure as well as the fields coupled into the output regions and into the substrate for typical devices. Power flow in the longitudinal and in the transverse directions in the structure is determined for the first time to our knowledge. Conservation of energy is observed for the reflected, air output, substrate coupled, and the forward fields.

2. APPROACH

2.1 Artificially period structure

The first step in the technique is to create an artificial periodic structure that can be analyzed by the rigorous coupled wave approach (RCWA) as has been previously proposed and implemented [3-5]. This is achieved by creating a unit cell for the device under consideration and constructing an infinitely periodic structure with the device unit cell as its

unit period. For the device under consideration shown in Fig. 2, the direction of periodicity of the artificial structure is perpendicular to the propagation direction of the guided mode in the device as shown in Fig. 3. As a result, the output coupled fields in air and in substrate regions remain within the artificial grating structures. To isolate each unit cell device within the structure, the artificial periodic structure's unit cell is constructed by adding two perfectly matching layers (PML) parallel to the structure one on the substrate side and the other located about one half wavelength above the grating coupler structure as shown in Fig. 4. The anisotropic magnetic properties of each of the two PML layers are designed (as will be discussed in sec. 2.2) such that at two interfaces the layers will be reflectionless at all angles, polarizations, and wavelengths. Therefore, all power is transmitted and contained in the PML. The thickness and loss properties of the PML are also designed such that all power is absorbed within the matching layer. This will insure electromagnetic isolation between each unit cell and the adjacent cells. Incorporating the PML sections in a typical structure, the unit cell width (grating period) is 4-6 light wavelengths.

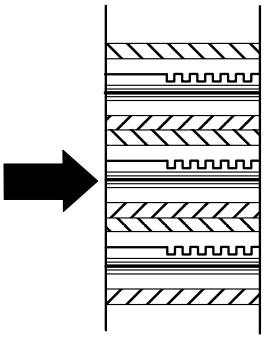

Fig. 3. Artificial Periodic Structure

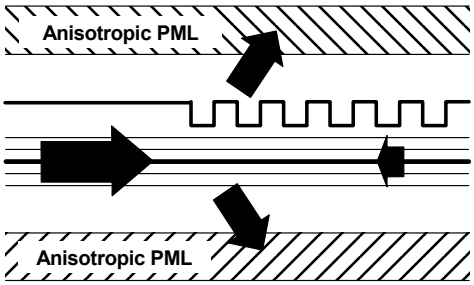

Fig. 4. Unit cell

This artificial but truly multi-layer periodic structure can then be analyzed efficiently and accurately using the RCWA to obtain a rigorous vector electromagnetic based solution of the diffraction problem. The formulation of the RWCA is revised to account for lossy anisotropic dielectric and magnetic properties of the PML layers.

2.2 Anisotropic perfectly matched layers (PML)

The perfect matching layer (PML) was introduced by Berenger [6] for truncating two-dimensional finite difference time domain (FDTD) meshes. Maxwell's equations were modified to add a new degree of freedom. This determines the permittivity and permeability of a lossy material layer such that field incident from the substrate region into the PML is totally transmitted and absorbed in the PML for all wavelengths, polarizations and angles of incidence. However, the implementation of the Berenger approach requires modifications of the Maxwell's equations, which in turn requires significant modification of the coupled-wave equations. Fortunately Sacks et. al. [7] presented an equivalent approach for determining the electromagnetic properties of the PML layer. The approach is based on using anisotropic material with complex permeability and permittivity properties to describe the PML layer. The complex permittivity and permeability tensors of the medium are chosen such that the interface is totally anti-reflective. Sacks's approach does not require modification of the Maxwell's equations and implementation is straightforward. According to Sacks et. al. the anisotropic properties of the PML matched to a homogenous region of refractive index is given by:

$$[\boldsymbol{\varepsilon}]_{PML} = n^2 [\boldsymbol{\mu}]_{PML}$$

$$[\boldsymbol{\mu}]_{PML} = \begin{bmatrix} \frac{1}{1-j\delta} & 0 & 0 \\ 0 & 1-j\delta & 0 \\ 0 & 0 & 1-j\delta \end{bmatrix}$$

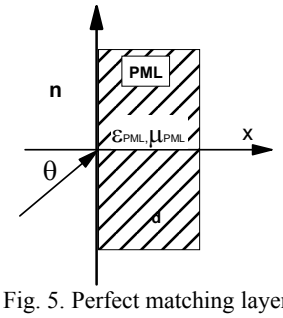

Fig. 5. Perfect matching layer

$[\varepsilon]$ and $[\mu]$ are the complex relative permittivity and relative permeability tensors of the PML layers. n is the refractive index of the non-magnetic input region. Note that the tensor describes a uniaxial material with the optic axis along the

normal to the boundary as shown in Fig. 5. The elements of the tensor along the normal to the boundary are the inverse of the other two equal components. At this interface, all of the energy will be transmitted to the PML at all wavelengths, polarizations, and angles of incidence. The normalized refracted field has the form:

$$E_t = e^{-k_0 n \delta \cos\theta z} e^{-jk_0 n(\sin\theta x + \cos\theta z)}$$

θ is the angle of incidence. The quantity δ does not impact the total transmission at the interface but it determines the absorption characteristics within the PML layer. It is selected to minimize the thickness of the PML layer to reduce computation time while maintaining slow enough absorption in the structure to insure that the PML performance is tolerant to deviation from the assumption of considering the interface between two half-space semi-infinite regions.

2.2 Coupled-wave equations for dielectric/magnetic anisotropic gratings

For anisotropic structures, the relative permittivity and relative permeability tensors are of the form:

$$[\boldsymbol{\varepsilon}] = \begin{bmatrix} \varepsilon_x & 0 & 0 \\ 0 & \varepsilon_y & 0 \\ 0 & 0 & \varepsilon_z \end{bmatrix} \quad \text{and} \quad [\boldsymbol{\mu}] = \begin{bmatrix} \mu_x & 0 & 0 \\ 0 & \mu_y & 0 \\ 0 & 0 & \mu_z \end{bmatrix}$$

The anisotropic magnetic properties of a grating impact the field interaction within the grating region and the coupled-wave equations must be revised accordingly. Following the approach and the notation presented in ref. [8] (and for grating periodicity in the x-direction and the normal to the boundary in the z-direction), the tangential fields in the grating are:

$$E_y = \sum_i S_{yi} e^{-jk_{xi}x}$$

$$H_x = -j\sqrt{\frac{\in_0}{\mu_0}} \sum_i U_{xi} e^{-jk_{xi}x}$$

$$k_{xi} = k_0 n \sin\theta - i\frac{2\pi}{L}$$

L is the grating period, θ is the angle of incidence, and k_0 is the wave number in free space. The revised formulation for the coupled wave equations is:

$$\frac{\partial^2 \mathbf{S}_y}{\partial z^2} = \left[\frac{1}{\boldsymbol{\mu}_x}\right]^{-1} \left[\mathbf{K}[\boldsymbol{\mu}_z]^{-1}\mathbf{K} - k_0^2[\boldsymbol{\varepsilon}_y]\right]\mathbf{S}_y$$

$$k_0 \mathbf{U}_x = \left[\frac{1}{\boldsymbol{\mu}_x}\right]\frac{\partial \mathbf{S}_y}{\partial z}$$

K is a diagonal matrix with element: k_{xi}. For TM polarization, the tangential field components in the grating region are:

$$H_y = \sum_i U_{yi} e^{-jk_{xi}x}$$

$$E_x = j\sqrt{\frac{\mu_0}{\in_0}} \sum_i S_{xi} e^{-jk_{xi}x}$$

The revised coupled wave equations for anisotropic magnetic media are:

$$\frac{\partial^2 \mathbf{U}_y}{\partial (k_0 z)^2} = \left[\frac{1}{\varepsilon_x}\right]^{-1} \left[\mathbf{K}[\mu_z]^{-1}\mathbf{K} - k_0^2[\mu_y]\right]\mathbf{U}_y$$

$$\mathbf{S}_x = \left[\frac{1}{\varepsilon_x}\right]\frac{\partial \mathbf{U}_y}{k_0 \partial z}$$

Note that proper expansion is used for the permittivity and permeability components in the direction of the periodicity to improve convergence [9]. Similar formulations have been presented in ref [5]. Other than the revision in the coupled-wave equations, the rest of the RCWA formulation for tangential field matching at the boundaries and calculation of the diffracted fields are unchanged.

2.3 Method for calculating of the field distribution and power flow within the structure

As mentioned, the revised coupled-wave equations may be solved using published techniques to determine the diffraction properties of the artificial gratings. However, there are two major challenges that must be addressed. First, the technique used in matching the tangential fields at the boundaries between the grating layers must allow for efficient, accurate, and stable calculation for all field components at any point within the structure. This will allow for calculating the output coupled field profile in air and in the substrate, as well as the corresponding power coupling efficiency. This can either be achieved using the enhanced transmittance matrix approach proposed by Moharam et al. [10] as reformulated by Tan [11] or the Scattering matrix approach [12, 13]. However, in the problem under consideration, the number of grating layers within the structure is extremely large. For example in a grating coupler length of 600 microns and a grating period of 300 nm, the number of grating periods is more than 4000 layers. This is coupled with an artificial grating structure with overall grating periods of 4-6 light wavelengths, and thus requires a large number of space harmonics to describe the field in the coupled structure. This makes the available transmittance or the S-matrix techniques, in their present form, extremely time consuming, and thus seriously limiting the usefulness of applying the grating theory technique to meso-scale grating coupler devices and other similar integrated optical devices. To illustrate this difficulty, we briefly review the fundamental formulation of the S-matrix approach described in detail in Ref. (12-13). In the S-matrix method, the forward diffracted field amplitudes and the backward diffracted field amplitudes are related to the incident field amplitudes by a scattering matrix. Considering a N-stack of grating layers as shown in Fig 6, the matrix is of the form:

$$\begin{bmatrix} \mathbf{b}_{N+1} \\ \mathbf{f}_0 \end{bmatrix} = [\mathbf{S}] \begin{bmatrix} \mathbf{0} \\ \mathbf{f}_{in} \end{bmatrix} = \begin{bmatrix} \mathbf{T}^b & \mathbf{R}^f \\ \mathbf{R}^b & \mathbf{T}^f \end{bmatrix} \begin{bmatrix} \mathbf{0} \\ \mathbf{f}_{in} \end{bmatrix}$$

The vectors $[\mathbf{b}_{N+1}], [\mathbf{f}_{in}]$, and $[\mathbf{f}_0]$ represent the backward reflected, incident, and forward diffracted field amplitudes respectively. The diffracted amplitudes are given by:

$$\mathbf{b}_{N+1} = \mathbf{R}^f \mathbf{f}_{in} \qquad \mathbf{f}_0 = \mathbf{T}^f \mathbf{f}_{in}$$

Each sub matrix in the S-matrix is of size $n \times n$ where n is the number of space harmonics retained in the field expansion.
The elements of the scattering matrix are given:

$$[\mathbf{S}] = [\mathbf{s}_N] * [\mathbf{s}_{N-1}] * \cdots * [\mathbf{s}_p] * \cdots * [\mathbf{s}_1] * [\mathbf{s}_0]$$

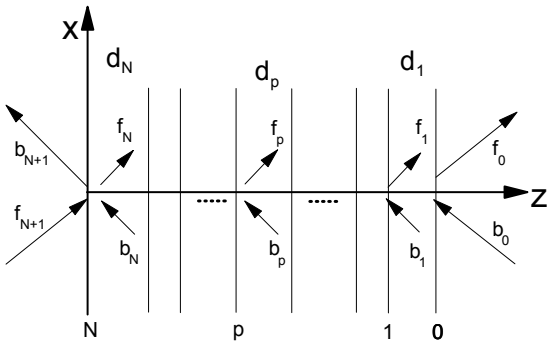

Fig. 6. Diffracted amplitudes in a layered grating

The " * " product is defined in ref 12. The elements of the S-matrix for each layer depend on the solution of the coupled-wave problem in the layer. For TE polarization, the solution is of the form:

$$\begin{bmatrix} \mathbf{S(z)} \\ \mathbf{U(z)} \end{bmatrix} = \begin{bmatrix} \mathbf{W} & \mathbf{W} \\ \mathbf{V} & -\mathbf{V} \end{bmatrix} \begin{bmatrix} \mathbf{e}^{\mathbf{q}(\mathbf{z}-\mathbf{L})} & \mathbf{0} \\ \mathbf{0} & \mathbf{e}^{-\mathbf{qz}} \end{bmatrix} \begin{bmatrix} \mathbf{b} \\ \mathbf{f} \end{bmatrix}$$

$$\mathbf{V} = [1/\mu_x]\mathbf{W}[\mathbf{q}]$$

where $[\mathbf{W}]$ and $[\mathbf{q}]$ are the eignevectors and the eigenvalues of the coupled wave equation above. [**b**] and [**f**] are the amplitudes of backward and forward harmonics. The S-matrix for the p-layer is given by:

$$\left[\mathbf{s}_p\right] = \begin{bmatrix} \mathbf{t}_p^b & \mathbf{r}_p^f \\ \mathbf{r}_p^b & \mathbf{t}_p^f \end{bmatrix}$$

Where

$$\mathbf{t}_p^b = 2\left[\mathbf{W}_p^{-1}\mathbf{W}_{p+1} + \mathbf{V}_p^{-1}\mathbf{V}_{p+1}\right]^{-1}\mathbf{X}_p$$
$$\mathbf{r}_p^f = \left[\mathbf{W}_p^{-1}\mathbf{W}_{p+1} + \mathbf{V}_p^{-1}\mathbf{V}_{p+1}\right]^{-1}\left[-\mathbf{W}_p^{-1}\mathbf{W}_{p+1} + \mathbf{V}_p^{-1}\mathbf{V}_{p+1}\right]$$
$$\mathbf{r}_p^b = \mathbf{X}_p\left[\mathbf{W}_{p+1}^{-1}\mathbf{W}_p + \mathbf{V}_{p+1}^{-1}\mathbf{V}_p\right]^{-1}\left[-\mathbf{W}_{p+1}^{-1}\mathbf{W}_p + \mathbf{V}_{p+1}^{-1}\mathbf{V}_p\right]\mathbf{X}_p$$
$$\mathbf{t}_p^f = 2\mathbf{X}_p\left[\mathbf{W}_{p+1}^{-1}\mathbf{W}_p + \mathbf{V}_{p+1}^{-1}\mathbf{V}_p\right]^{-1}$$
$$\mathbf{X}_p = \left[e^{-q_p d_p}\right]$$

The overall S-matrix for the stack is obtained by constructing the S-matrix for each grating layer and then using the special "*" product formulation. The forward and backward diffracted field amplitudes outside the grating structure are then calculated as discussed above. In general the S-matrix is not symmetric. For a grating structure with a very large number of layers (N), the execution time and the required computer memory could be prohibitive since constructing the S-matrix for each layer requires four $n \times n$ matrix inversions and each star multiplicate requires two $n \times n$ matrix inversions for a total of 8N $n \times n$ matrix inversions for the structure. For example, in the problem under consideration the number of grating layers could run to 4000 rendering this approach impracticable. However, taking note of the periodic repetitive nature of the coupler, one can construct an S-matrix for one grating period, using this unit cell to construct the overall S-matrix, thereby reducing the number of matrix inversions to 2N or less. This is still a large number of matrix inversions but that might be acceptable.

The main limitation of the S-matrix approach is the cost involved in determining the fields within the structure. The field amplitudes must be calculated at each interface between the layers within the structure, and those amplitudes are used to calculate each of the space harmonics ($\left[\mathbf{S}\right]$ and $\left[\mathbf{U}\right]$) at the interface. The total field is then calculated by summing the space harmonics at all points at the interface. The power flow density is then determined from the Poynting's vector:

$$< \mathbf{P} >= 0.5\,\mathrm{Re}\left[\mathbf{E} \times \mathbf{H}^*\right]$$

To determine the field amplitudes at an interface/plane (e.g. the p-th interface), the backward and forward field amplitudes at two interfaces on either side of the plane must be known. The relevant formulation is used:

$$\mathbf{f}_p = \left[\mathbf{1} - \mathbf{R}_L^b\mathbf{R}_R^f\right]^{-1}\left[\mathbf{R}_L^b\mathbf{T}_R^b\mathbf{b}_R + \mathbf{T}_L^f\mathbf{f}_L\right]$$
$$\mathbf{b}_p = \mathbf{T}_R^b\mathbf{b}_R + \mathbf{R}_R^f\mathbf{f}_p$$

$\mathbf{f}_L$ and $\mathbf{b}_R$ are the forward field amplitude at the left interface and the backward field amplitude at the right interface. The S-matrices are :

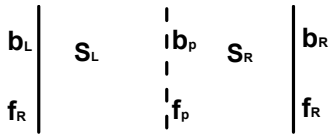

Fig. 7. Field amplitudes within the structure

$$\left[\mathbf{S}_R\right] = \begin{bmatrix} \mathbf{T}_R^b & \mathbf{R}_R^f \\ \mathbf{R}_R^b & \mathbf{T}_R^f \end{bmatrix} = \begin{bmatrix} \mathbf{t}_p^b & \mathbf{r}_p^f \\ \mathbf{r}_p^b & \mathbf{t}_p^f \end{bmatrix} \cdots * \cdots \begin{bmatrix} \mathbf{t}_0^b & \mathbf{r}_0^f \\ \mathbf{r}_0^b & \mathbf{t}_0^f \end{bmatrix}$$
$$\left[\mathbf{S}_L\right] = \begin{bmatrix} \mathbf{T}_L^b & \mathbf{R}_R^f \\ \mathbf{R}_L^b & \mathbf{T}_L^f \end{bmatrix} = \begin{bmatrix} \mathbf{t}_N^b & \mathbf{r}_N^f \\ \mathbf{r}_N^b & \mathbf{t}_N^f \end{bmatrix} \cdots * \cdots \begin{bmatrix} \mathbf{t}_{p+1}^b & \mathbf{r}_{p+1}^f \\ \mathbf{r}_{p+1}^b & \mathbf{t}_{p+1}^f \end{bmatrix}$$

That means constructing two S-matrices: one for all the layers to the right of the interface and one for all layers on the left side of interface as shown in Fig. 7. This has to be repeated at each interface which limits utilization of the previously calculated S-matrices. This is truly where the S-matrix approach, in its present form, is practically unusable to determine the nano-scale field distribution within hundreds of microns long structures.

2.4 Efficient Scattering matrix approach for Grating Structures

In addressing the almost fatal limitation for the problem under consideration, we have developed a very efficient implementation of S-matrix that takes advantage of the periodicity of the grating structure. This approach practically eliminates the prohibitively time consuming problem discussed in the previous section. The developed technique involves several components each of which contributes to the overall efficiency of the method.

2.4.1 Homogenous zero-thickness layers at each interface.

The first component of the new approach is to add two identical zero-thickness isotropic homogenous uniform regions (of arbitrary refractive index, preferably the input region index) on either side of each layer with the structure as shown in Fig. 8. The S-matrix for the composite symmetric layer is:

$$[\mathbf{s}] = \begin{bmatrix} 4\mathbf{DX}\left[\mathbf{I}-\mathbf{B}^2\right]^{-1}\mathbf{A} & \mathbf{C}+4\mathbf{DXB}\left[\mathbf{I}-\mathbf{B}^2\right]^{-1}\mathbf{A} \\ \mathbf{C}+4\mathbf{DXB}\left[\mathbf{I}-\mathbf{B}^2\right]^{-1}\mathbf{A} & 4\mathbf{DX}\left[\mathbf{I}-\mathbf{B}^2\right]^{-1}\mathbf{A} \end{bmatrix}$$

where

$$\mathbf{A} = \left[\mathbf{V}+\mathbf{QW}\right]^{-1}\mathbf{Q}$$
$$\mathbf{B} = \left[\mathbf{V}+\mathbf{QW}\right]^{-1}\left[\mathbf{V}-\mathbf{QW}\right]\mathbf{X}$$
$$\mathbf{D} = \mathbf{W}\left[\mathbf{V}+\mathbf{QW}\right]^{-1}\mathbf{V}$$
$$\mathbf{C} = -\mathbf{W}\mathbf{A}^{-1}\mathbf{B}\mathbf{W}^{-1}$$
$$\mathbf{Q} = diag[\mathbf{q_i}] \qquad q_i = \sqrt{k_{xi}^2 - n^2}$$

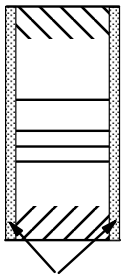

Fig. 8 Symmetric unit layer

$[\mathbf{W}]$, $[\mathbf{V}]$ and $[\mathbf{X}]$ are as defined in sec 2.3. , The eigenvector matrix in the uniform region is a unity matrix, and the eigenvalues are directly calculated from the dispersion relation in the uniform region. n is the refractive index of the homogenous regions. By introducing those two uniform zero-thickness layers, we significantly improve the computation efficiency on several fronts. First the new artificial composite structure is truly symmetric and the S-matrix for this composite structure is symmetric thus reducing the computation time and memory requirement by a factor of 2. Second, it is much more efficient to calculate the field distribution and the power flow within this homogenous uniform zero-thickness layer than within an inhomogeneous grating region since the field is a uniform region composed of truly simple plane waves. In fact the field components in this uniform region are:

$$S_i = b_i + f_i$$
$$U_i = q_i\left(b_i - f_i\right)$$

This is a significant saving in execution time with almost insignificant effort to construct the composite S-matrix. Therefore, we strongly recommend that this improvement should be built-in for the general S-matrix approach since it is very easily incorporated and results in significant improvement in calculation efficiency under all circumstances.

2.4.2 Symmetric grating unit cell

The second component of the new approach is to construct a symmetric composite layer of one full grating coupler period. This is achieved by creating a composite unit cell from a cell (including zero-thickness uniform layers) of the grating coupler layer that has the grating groove between two identical layers of grating coupler layer that are composed of the grating ridge as shown in Fig. 9. The representation results in a symmetric structure with symmetric S-matrices. In addition the composite S-matrix of any number of full grating periods (e.g. N) is also symmetric

$$\begin{bmatrix} \mathbf{t_c} & \mathbf{r_c} \\ \mathbf{r_c} & \mathbf{t_c} \end{bmatrix} \cdots * \cdots \begin{bmatrix} \mathbf{t_c} & \mathbf{r_c} \\ \mathbf{r_c} & \mathbf{t_c} \end{bmatrix} \cdots * \cdots \begin{bmatrix} \mathbf{t_c} & \mathbf{r_c} \\ \mathbf{r_c} & \mathbf{t_c} \end{bmatrix} = \begin{bmatrix} \mathbf{t} & \mathbf{r} \\ \mathbf{r} & \mathbf{t} \end{bmatrix}_N$$

This formulation results in reducing the numerical computation and memory requirement by a factor of 2. In addition, we use a binary multiplication scheme of the form :

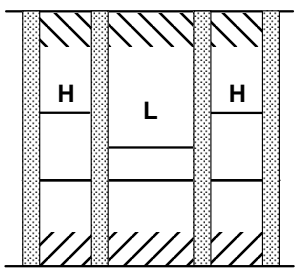

Fig. 9. Symmetric unit grating cell

$$[S]_2 = [s] * [s]$$
$$[S]_4 = [S]_2 * [S]_2$$
$$\vdots$$
$$[S]_N = [S]_{(N/2)} * [S]_{(N/2)}$$

The number of " * " products is then reduced from **N** to $\log_2 N$. That is for a structure of over 2,048 grating periods, the number of " * " products can be reduced from **2,048** to an amazing **11** products. This is a more than two order of magnitude improvement in the computation efficiency which makes this reformulated S-matrix approach an extremely useful technique. If the case of chirped grating coupler or couplers with multiple periodic sections is considered, the formulation can be applied locally with still tremendous improvement in the computation efficiency.

2.4.3 Binary approach in calculating the field distribution with the structure

The third component in efficient implementation of the S-matrix approach is in calculating the field amplitude at an interface/plane within the structure. As discussed in sec. 2.3, determining the field amplitudes requires knowledge of the field amplitudes at two interfaces on each side of the interface and requires constructing the S-matrices to the right and left of the interface. This requires repeated (N times) calculation of two S-matrices which is extremely time consuming. In our implementation, we construct a binary scheme to drastically improve the efficiency of the calculation. We select a length of the coupler such that the number unit cells $N = 2^M$ where M is an integer and it is large enough that all energy is coupled out of the structure. In practice there is no loss of generality since an artificially added length is inconsequential to the problem. The procedure for the determining the field amplitudes within the structure is as follows. First the transmitted and reflected field amplitudes for the entire structure are determined using the S-matrix approach with improved implementation described in sec. 2.4.1 and 2.4.2. The field at the interface located halfway in the structure is calculated as illustrated shown in Fig. 10.

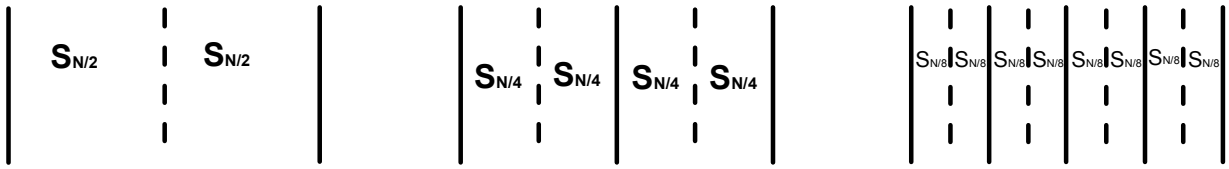

Fig. 10. Binary scheme for determining field amplitudes within the structure

This requires calculating one symmetric S-matrix $[S]_{N/2}$ since the left and right S-matrices are identical. The values of the field amplitudes at the half-way interface is used along with the field amplitudes at the two outside interfaces to calculate the fields at the one quarter and three quarter interfaces within the structures. This again requires constructing one symmetric $[S]_{N/4}$. This binary scheme is repeated to calculate the field amplitudes at four interfaces with one S-matrix construction $[S]_{N/8}$ and so on. This scheme results in M S-matrices rather than 2N S-matrices (recall $N = 2^M$). This is a tremendous saving in computation efficiency and computer memory requirements. This very efficient implementation makes it possible to rigorously solve Maxwell's equations to determine the nano-scale full field spatial distribution and power flow distribution in a grating coupler of several hundreds of microns length in less than 30 seconds on a desktop/ laptop personal computer.

3. RESULTS

To demonstrate the technique and its extreme efficiency, an $Al_xGa_{1-x}As$ semiconductor grating coupler structure is analyzed. The device has gain $Al_xGa_{1-x}As$ multi quantum well region of few nanometers thick between two graded passive Al_xGa_{1-x} regions for mode confinement on a GaAs substrate. The nature of the semiconductor laser/amplifier produces a TE polarized mode. The grating coupler is etched in the top cladding region with periodicity of 275-325 nm, grating depth of 200-300 nm. The grating coupler is 500-1000 microns long and is detuned to minimize the reflection back into the laser/amplifier section. The graded anisotropic magnetic perfect matching layer of 250 nm thickness obtained through an optimization scheme is used. However, a single 500 nm thick layer with $\delta = 0.9$ produced almost identical results. Two hundred diffracted orders are used in the field expansion. The execution time using 2.5GHz

Pentium 4 PC with 2G RAM (Windows XP) is less than 30 seconds to determine the field distribution and power flow of the out-coupled beams and within the grating coupler structure.

Figure 11 shows the power flow in the structure for the longitudinal direction. Note the light scattering at the transition between the uniform waveguide structure and the grating section of the waveguide due to mode mismatch in the two sections. Figure 11(a) shows the longitudinal power flow near the discontinuity. The modulation of the field distribution in the uniform waveguide section is a result of interference of the forward wave with the reflected field at the waveguide/grating discontinuity interface. The longitudinal power flow in the grating section is decreasing exponentially as energy is coupled out of the device.

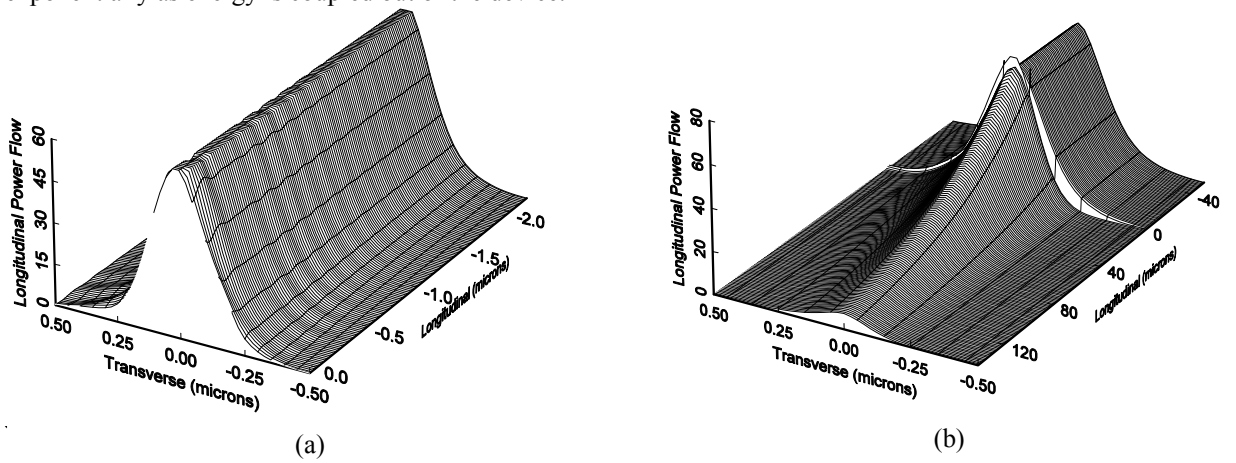

Fig. 11. Longitudinal power flow near the waveguide/coupler interface and in the whole device

Figure 12 shows the power flow in the transverse direction in the grating coupler structure. Again, note the light scattering at the transition between the uniform waveguide structure and the grating section of the waveguide due to mode mismatch in the two sections. Figure 12(a) shows the longitudinal power flow near the discontinuity. The modulation of the field distribution in the uniform waveguide section is a result of interference of the forward wave with the reflected field at waveguide/grating discontinuity interface and of the light scattering at the interface. The transverse power flow in the grating section is decreasing in an exponentially like manner since the energy in the coupler is being depleted and there is less energy to be out-coupled.

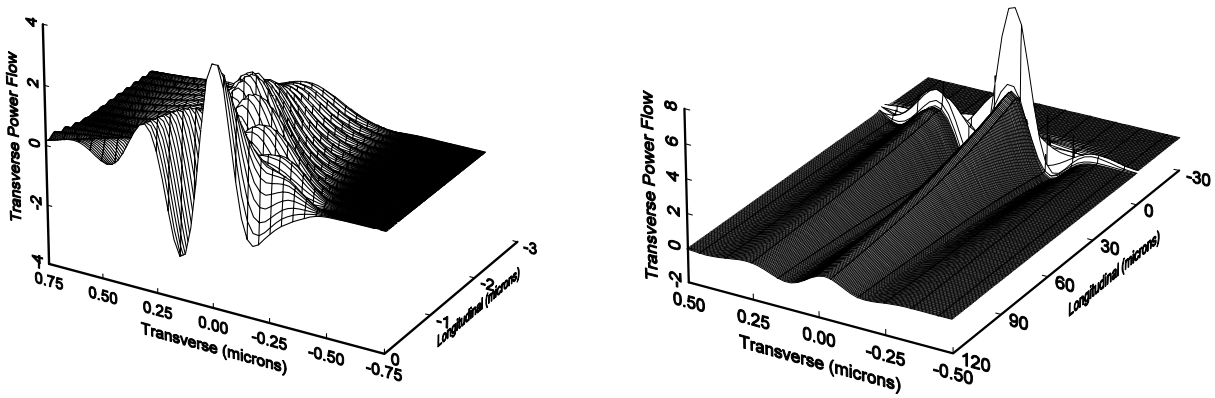

Fig. 12. Transverse power flow near the waveguide/coupler interface and in the entire device

It is important to note that in all of our calculations, power is conserved. This is determined by integrating the power entering a closed surface and the power exiting the surface in the direction normal to the surface as shown in Fig. 13.

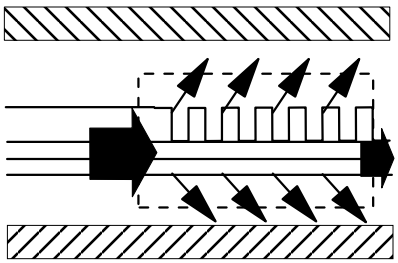

Fig. 13. Power conservation in the grating coupler

The normal power distribution of the out-coupled beams in air and in the substrate regions are shown in Fig. 14. For the parameters used in the calculation there is slightly more energy coupled in the substrate side than the air side. The observed oscillations in the beam profile in the substrate are the result of the interferometric effects, since no antireflective layer is used.

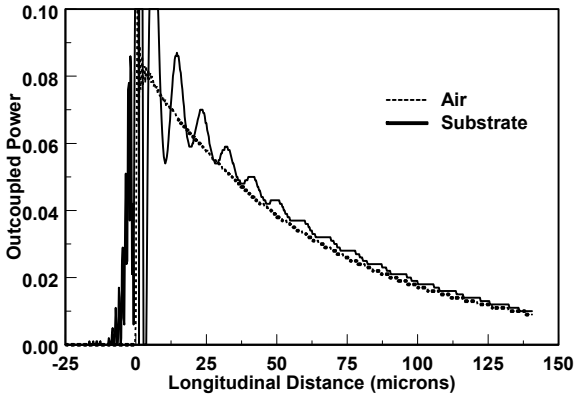

Fig. 14. Output-coupled power and beam intensity profile

These calculated examples demonstrate that the technique is extremely powerful in determining the electromagnetic fields, and therefore, the power flow distribution, over nanoscale dimensions and near discontinuities. It is important to note that in all of our calculations, power is conserved.

4. SUMMARY

We presented an extremely efficient rigorous vector electromagnetic analysis of field distribution and power flow in grating coupled surface emitting structures. These structures have high index contrast (n=3.3), small grating period (~300 nm), large grating depth (250nm), and a long grating coupler (500-1000 microns). Accurate modeling of this type of structure requires a technique that is based on the exact solution of the vector Maxwell's equations and full vector electromagnetic representation of the optical field distribution in the structure. The long length of the grating coupler and small features (~150 nm) of the grating render standard analysis techniques that are based on the calculation of electromagnetic fields on a spatial grid such as finite difference time domain (FDTD) method, prohibitively inefficient for these structures. The developed technique is based on constructing an artificially periodic structure of identical grating coupled device cells separated by anisotropic magnetic/electric perfect matching layers. The resulting periodic multi-layered structure is analyzed using the RCWA. A very efficient implementation of the S-matrix recursive approach is developed to overcome the numerical inefficiency associated with 6,000 layers in the grating structure. Calculated field distribution, mode structure, and output coupled fields are presented. Execution time using a 2.5 GHz Pentium 4 PC is less than 30 seconds. We present calculated distributions of all the electric and magnetic field components within the structure as well as the fields coupled into the output regions and into the substrate for typical devices. Field distribution and power flow in the longitudinal and in the transverse directions in the structure are determined for the first time to our knowledge. Conservation of energy is observed for the reflected, the air and substrate coupled, and the forward fields

REFERENCES

1. G. A. Evans, N. W. Carlson, J. M. Hammer, and J. K. Butler, in " Surface emitting semiconductor lasers and arrays," G. A. Evans and J. Hammer, Eds. 119-216 Academic Press, (1993).
2. Larsson, N. Ericksson, A. Kristjansson, P. Modh, M. Uemukai, T. Suhara, and H. Nishihara, "Grating-coupled surface emitters," in Proceedings of Testing, Packaging, and reliability of semiconductor lasers IV, SPIE Vol. **3626**, 190 (1999).
3. P. Vahihama and J. Turunen, Diffractive Optics and Micro Optics, Technical Digest Optical Society of America, Washington, D. C., **10**, 69-72 (1998).
4. Ph. Lalanne and E. Silberstein, "Fourier modal method applied to waveguide computation problems," Opt. Lett, **25**, 1092-1094 (2000).
5. E. Silberstein, P. Lalanne, J-P Hugonin, and Q. Cao," Use of grating theories in integrated optics," J. Op. Soc. Am. A, **18**, 2865-2875 (2001).
6. J-P Berenger, "A perfectly matched layer for the absorption of electromagnetic waves," J. Comp. Phys.,**114**, 185-200, (1994).
7. Z. S. Sacks, D. M. Kingsland, R. Lee, and J. F. Lee, "A perfect matched anisotropic absorber for use as an absorbing boundary condition," IEEE Antennas Prop. Trans. **43**, 1460-1463 (1995).
8. M. G. Moharam, E. B. Grann, D. A. Pommet, and T. K. Gaylord " Formulation for stable efficient implementation of the rigorous coupled wave analysis of binary gratings, J Opt. Soc. Am **12**, 1068-1076 (1995).
9. Ph. Lalanne, G. M. Morris, "Highly improved convergence of the coupled-wave method for TM polarization," J. Opt. Soc. Am A **13**, 779-784 (1996).
10. M. G. Moharam, D. A. Pommet, E. B. Grann, and T. K. Gaylord "Stable implementation of the coupled wave analysis for surface relief gratings: enhanced transmittance approach," J Opt. Soc. Am **12**, 1077-1786 (1995).
11. E. L. Tan, "Notes on the formulation of the enhanced scattering transmittance matrix approach," J. Opt. Soc. Am. A **20**, 1157-1161 (2003).
12. N. P. K. Cotter, T. W Preist, and J. R. Sambles, "Scattering matrix approach to multilayer diffraction," J. Opt. Soc. Am. A 12, 1097-1103 (1995).
13. L Li, "Formulation and comparison of two recursive matrix algorithms for modelling layered diffraction gratings," J. Opt. Soc. Am A, vol **13**, 1024-1035 (1996).